15.3 TTUKa Mobile Doppler Radar Observations of Near-Surface Circulations in VORTEX2

Patrick S. Skinner,* Christopher C. Weiss, Anthony E. Reinhart, William S. Gunter, John L. Schroeder and Jerry Guynes
Texas Tech University, Lubbock, Texas

1. INTRODUCTION

The 2010 campaign of the second Verification of the Origin of Rotation in Tornadoes Experiment (VORTEX2) marked the first time two Ka-band mobile Doppler radars developed by Texas Tech University (TTUKa) (see Weiss et al. 2009 for TTUKa specifications) deployed in tandem in a severe storm environment. The TTUKa radars achieve a very high azimuthal and range resolution by coupling a narrow beamwidth with non-linear frequency modulation, providing a range resolution consistent with a short pulse duration without sacrificing the sensitivity of a longer pulse. The ability of the TTUKa radars to resolve small-wavelength phenomena in supercells supported a primary research mission of observing near-surface tornadic and pre-tornadic circulations and surrounding storm-scale features in VORTEX2.

Data presented herein will focus on two datasets obtained during the 2010 VORTEX2 campaign, a long-term, short-baseline dual-Doppler deployment within a pre-tornadic, high-precipitation supercell occurring on 18 May 2010 near Dumas, Texas, and a single-Doppler dataset of a weakly tornadic supercell southwest of Limon, Colorado on 11 June 2010. Both cases exhibit multiple "surges" within the rear-flank downdraft (RFD) and a multiple RFD gust front (RFGF) structure. The RFD surges are observed with a higher frequency than previously documented, with three distinct surges identified over an approximately seven minute span in the Dumas supercell. Three RFD surges are also observed over a six minute span in the Limon supercell. In both cases small circulations develop at the apex of internal RFD surges, with a brief, nontornadic vortex forming in the Dumas supercell and two weak tornadoes in the Limon supercell.

Corresponding author address: Patrick S. Skinner, Texas Tech University, Wind Science and Engineering Department, Lubbock, TX, 79409; e-mail: Patrick.Skinner@ttu.edu

2. METHODOLOGY

2.1. 18 May 2010

Dual-Doppler data were collected by the TTUKa radars from 2254 – 2324 UTC along the Hartley-Moore county line east of Dumas, TX as a pre-tornadic, high precipitation supercell passed to the north (Fig. 1). Data were collected at 0.0, 0.25, and 0.5° elevation angles; however, this study will limit syntheses to 0.0° elevation scans, providing a two-dimensional representation of the near-surface wind field. The dual-Doppler deployment was conducted with a 3.3 km baseline, which corresponds to a range from either radar (R_m) of 6.37 km for a 30° crossing angle. The range resolution of the TTUKa radars is approximately 35 m and a 0.49° beamwidth corresponds to azimuthal resolution of 54.5 m at R_m. Based, on these values, a small grid spacing of 50 m was chosen for the objective analysis of the radar data.

Prior to objective analysis and dual-Doppler synthesis, initial quality control was applied to each radar scan to remove erroneous data. The orientation of each scan was corrected by matching ground clutter patterns such as road intersections to their geographic location. This procedure had the additional effect of removing "jitter" introduced by the radar processing software at periods of antenna acceleration at the beginning of each sector scan. The Solo II processing software was used to subjectively unfold aliased velocity data, remove range-folded data, and remove erroneous returns due to ground clutter.

Objective analysis and subsequent dual-Doppler synthesis were performed using the REORDER and CEDRIC software available from the National Center for Atmospheric Research (NCAR). The objective analysis method and smoothing parameters were chosen to limit the amount of smoothing applied and retain small-scale features. A Barnes scheme was chosen with a κ value of 0.0029 km^2, radius of influence (R_c) of 0.122 km, and attenuation factor (α) of -15. These values result in a

Barnes response function of approximately 0.50 to phenomena with wavelengths of 200 m.

2.1. 11 June 2010

A single-Doppler dataset collected by TTUKa-2 is utilized for analysis of the 11 June case. TTUKa-2 deployed on HWY 24 approximately 20 km southwest of Limon from 23:20 to 23:44 UTC, capturing the genesis and the full lifecycle of two circulations, one of which designated as a weak tornado, as they passed to the north of the radar while scanning at 0.0° elevation. Similarly to the Dumas case, data from the Limon case was reoriented, de-aliased, and clutter-corrected using the Solo II software. Data were then objectively analyzed using the Cappi processing software utilizing a bilinear interpolation scheme with a grid spacing of 50 m. Though bilinear objective analysis schemes have been found to induce erroneous waveforms at long distances from the radar (Trapp and Doswell 2000), the proximity to the radar in this case should limit error introduced by the interpolation scheme (Tanamachi et al. 2006).

3. ANALYSIS

3.1. 18 May 2010

Eight dual-Doppler syntheses are considered over the period 23:00:02 to 23:06:30 UTC (Figs. 2-5). The analysis takes place after the initial RFGF has passed through the dual-Doppler domain. The region behind the initial RFGF is characterized by relatively light westerly and southwesterly winds, generally less than 20 m s^{-1} (Fig. 2a). However, two internal RFGFs (surge A, surge B) are observed across the western portions of the domain. Both surges are demarcated by areas of enhanced convergence along their RFGF and broad divergence within the surges themselves (Fig. 2b, 2e). Wind speeds within surge A are approximately 20-30 m s^{-1} and upwards of 40 m s^{-1} within surge B. Roughly one minute later, surge B has wrapped cyclonically around a broad surface circulation in the light winds north of the RFD surge (Fig. 2f) and is approaching the RFGF of the first surge. Over the following two minutes, the eastern extent of surge A becomes indistinct, while a strong east-west oriented convergence line sets up along its southern extent (Figs. 3b, 3e). Surge B continues to advance towards the RFGF of the first surge and an approximately 1 km in diameter, closed circulation develops north of its apex by 23:02:41 UTC (Fig. 3f).

The leading edge of surge C can be observed in the extreme northwest corner of the analysis domain at 23:02:41 UTC (Fig. 3d). Surge C generally follows the path of surge B over the following two analyses, wrapping cyclonically around the broad circulation at 23:03:26 (Fig. 4a). However, the circulation tightens to a small, intense vortex at the apex of surge C by 23:04:15 with a delta-V of approximately 75 m s^{-1} over a roughly 200 m span (Fig. 4d) and vertical vorticity values of 0.2 s^{-1} (Fig. 4f). Though this vortex could be considered a tornado, the compendious nature of the circulation (a low-reflectivity “eye” was only observed for a single scan in TTUKa-1 data) has led this case to be classified as one of tornadogenesis failure. However, it is noted that there is considerable ambiguity between weakly tornadic and nontornadic vortices. Also of note at 23:04:15 is the distinct line of convergence and cyclonic vertical vorticity located on the northern boundary of surge C. The boundary position between strong RFD winds and lighter winds north of the circulation resembles a smaller-scale version of boundaries produced by numerical simulations to the north and northwest of low-level mesocyclones (Wicker and Wilhelmson 1995; Adlerman et al. 1999; Beck and Weiss 2008).

Elsewhere in the domain at 23:04:13, surge B has developed a more southward component to its propagation and has completely overtaken surge A, reinforcing the east-west convergence line at the RFGF (Fig. 4d, 4e). The wind speed behind surge B has decelerated from 23:03:26 with values greater than 30 m s^{-1} only existing in a narrow region immediately behind the RFGF (Fig. 4d). By 23:05:30, the vortex has dissipated into an open region of cyclonic curvature in the wind field (Fig. 5a) and the leading edge of surge C is beginning to overtake the remnant RFGF from surges A and B. At 23:06:30, the three RFD surges have merged into a single internal RFGF with strong convergence along its leading edge and broad divergence within the downdraft. Additionally, winds have decelerated to less than 30 m s^{-1} throughout the analysis domain and no additional RFD surges are apparent.

3.2. 11 June 2010

The progression of three distinct RFD surges within the Limon supercell can be seen in

a series of four objectively analyzed, single-Doppler scans from TTUKa-2 (Fig. 6). The initial scan taken at 23:32:33 UTC shows the leading edge of the RFD approaching the position of TTUKa-2 at a range of approximately 4 km. Behind the initial RFGF, a secondary RFGF (surge B) is noted at a range of 8 km and is marked by a significant acceleration of the radial inflow from 15 - 20 m s^{-1} to greater than 30 m s^{-1} (Fig. 6a). A surface circulation is observed north of the apex of surge B (vortex B) at the inbound/outbound interface of the RFD surge and storm inflow. Two minutes later (Fig. 6b), the initial RFGF has progressed to within 3 km of TTUKa-2, while the RFGF of surge B has become well defined at a range of 6 km. The circulation north of the apex of surge B remains on the interface of the inbound/outbound returns and has intensified from the prior scan. Subtle evidence of a third surge is apparent at a range of approximately 9 km, with a second circulation developing north of the apex of surge C (vortex C). Like vortex B, this circulation is located at the inflow/outflow interface within the storm. By 23:36:33 (Fig. 6c), winds behind surge B have decelerated significantly, but the vortex to the north of the surge has intensified. Additionally, surge B has propagated ahead of the vortex, which is now well behind the apex of surge B and within 2 km of vortex C. Surge C is better defined than in the previous scan and the vortex north of its apex has also intensified to greater than 65 m s^{-1} gate-to-gate shear in raw radial velocity returns. Unlike vortex B, the trailing vortex remains just north of the apex of surge C with the maximum radial velocities observed in the scan just to its southwest. The final analysis period (Fig. 6d) shows the initial RFGF past the position of TTUKa-2, with the RFGF of surge B is barely distinguishable. The vortex associated with surge B has propagated to the north and retrograded, wrapping cyclonically around the stronger vortex C into the area of attenuation. The vortex north of the apex of the now well-defined surge C has further intensified to greater than 70 m s^{-1} in gate-to-gate shear and has become detached from the interface of storm inflow and outflow and resides fully within the storm RFD. Subsequent scans reveal the remnants of vortex B merge into vortex C as it reemerges from storm outflow and rapidly weakens. Both vortices show considerably weaker shear signatures by 23:41 UTC.

Like the vortex observed within the Dumas supercell, the vortices observed in the Limon storm present a classification problem as they could be interpreted as either tornadic or nontornadic. As a tornado was observed visually by storm spotters and a cohesive low-reflectivity “eye” was observed for a period greater than four minutes associated with vortex C it has been classified as a weak tornado. The less intense, shorter-lived vortex B is being considered a nontornadic circulation similar to the one observed within the Dumas supercell.

4. DISCUSSION

Several recent dual-Doppler studies have identified a dual RFGF structure in tornadic supercells (Wurman et al. 2007; Marquis et al. 2008a; Marquis et al. 2008b). Each of these studies identified a single internal RFD surge which wrapped cyclonically around the low-level vorticity maximum with time and persisted throughout the analysis. Additionally, some secondary RFGFs were found to be pendant to the tornadic circulation, which resided entirely within the broader-scale RFD outflow (Marquis et al. 2008b). This suggests that air parcels from within the internal RFD are entering the tornado and can play a role in tornado genesis, maintenance, and demise.

A unique finding to this study is the presence of multiple RFD surges within a single supercell at a single time. Additionally, the time-frame on which the RFD surges evolve is considerably faster than previously documented. In both supercells studied, the lifecycle of RFD surges was less than 10 minutes, with multiple surges initiating and wrapping cyclonically around a near-surface vorticity maxima prior to the dissipation of a prior surge. Though dual-Doppler syntheses are not available through a sufficient depth of the storm to diagnose the origin of the downdrafts responsible for internal RFD development, it is noted that the RFD surges qualitatively resemble occlusion downdrafts produced in numerically simulated supercells (Rotunno and Klemp 1985; Wicker and Wilhelmson 1995). The occlusion downdraft was found to be triggered in simulated supercells by a downward-directed vertical pressure gradient force induced by lowering pressures within a developing near-surface circulation (Wicker and Wilhelmson 1995). If the forcing for RFD surges observed within this study is similar to those of occlusion downdrafts, it is plausible that the rapid evolution and decay of the RFD surges observed is a reflection of the relatively weak surface circulations associated with them. It is noted that longer-lived RFD

surges presented in Marquis et al. 2008b were all associated with longer-lived, more intense surface circulations than those observed in this study.

A second finding unique to this study is that RFD surges were found to precede near-surface vortex intensification. Each intense near-surface vortex observed in this study developed north of the apex of an RFD surge. Though prior studies have documented RFD surges that developed after tornadogenesis and likely affected tornado maintenance (Marquis et al. 2008b), the development of an RFD surge pendant to a broad, near-surface circulation prior to vortex intensification suggest that RFD surges may play a role in tornadogenesis as well. However, an RFD surge is not a sufficient condition for tornadogenesis, as evidenced by the fact that several RFD surges documented did not produce intense near-surface rotation.

Several recent in situ studies have observed thermodynamic deficits within an RFD surge that are both warmer (Finley and Lee 2004; Lee et al. 2004; Karstens et al. 2010) and cooler (Skinner and Weiss 2008) than the broader RFD. As tornadoes have been shown to be more likely in supercells containing relatively warm RFDs (Markowski et al. 2002), it is possible that the ability of surface circulations on the apex of an internal RFD to develop and intensify is related to the thermodynamic characteristics within the RFD surge.

5. RECOMMENDATIONS

While multiple elevation scans exist for the Dumas case, they do not extend beyond 0.5° in elevation. Therefore, it is unlikely that the dual-Doppler synthesis will be able to capture the origin of downdrafts responsible for RFD surges. In order to identify the origin of RFD surges and discern potential forcing mechanisms, multiple Doppler analyses utilizing additional assets from VORTEX2 or assimilation of TTUKa data into a three-dimensional numeric simulation of the Dumas supercell will need to be undertaken.

In situ observations within both the RFD surges and broader scale RFD would allow differing thermodynamic character between storms and, potentially, successive RFD surges to be identified. Observations of distinct thermodynamic characteristics within each individual RFD surge would offer insight into the development of vortices near the apex of some surges, but not others.

Finally, analysis of two supercells, one nontornadic, one weakly tornadic, have been presented. Analysis of many more cases across the spectrum from nontornadic to strongly tornadic are required to fully access the prevalence and relationship, if any, to tornadogenesis and maintenance of RFD surges.

6. ACKNOWLEDGEMENTS

This research is supported by NSF Grant AGS-0964088. The authors wish to thank Brian Hirth, Ryan Metzger and Robin Tanamachi for their assistance with data processing and visualization. Amanda Thibault, Rich Krupar, and Trevor Boucher are acknowledged for their assistance with TTUKa data collection.

6. REFERENCES

Adlerman, E.J., K.K. Droegemeier, and R. Davies-Jones, 1999: A numerical simulation of cyclic mesocyclogenesis. *J. Atmos. Sci.*, **56**, 2045-2069.

Beck, J.R. and C.C. Weiss, 2008: The effects of thermodynamic variability on low-level baroclinity and vorticity within numerically simulated supercell thunderstorms. Preprints, *24th Conf. on Severe Local Storms*, Savannah, GA, *Amer. Meteor. Soc.*, 15.4

Finley, C.A. and B.D. Lee, 2004: High resolution mobile mesonet observations of RFD surges in the June 9 Basset, Nebraska supercell during Project ANSWERS 2003. Preprints, *22nd Conf. on Severe Local Storms*, Hyannis, MA, *Amer. Meteor. Soc.*, P11.3.

Karstens, C.D., T.M. Samaras, B.D. Lee, W.A. Gallus, and C.A. Finley, 2010: Near ground pressure and wind measurements in tornadoes. *Mon. Wea. Rev.*, **138**, 2570-2588.

Lee, B. D., C. A. Finley, and P. Skinner, 2004: Thermodynamic and kinematic analysis of multiple RFD surges for the 24 June 2003 Manchester, South Dakota cyclic tornadic supercell during Project ANSWERS 2003. Preprints, *22nd Conf. on Severe Local Storms*, Hyannis, MA, *Amer. Meteor. Soc.*, P11.2

Markowski, P.M., J.M. Straka, and E.N. Rasmussen, 2002. Direct surface thermodynamic observations within the rear-flank downdrafts of nontornadic and tornadic supercells. *Mon. Wea. Rev.*, **130**, 1692-1721.

Marquis, J., Y. Richardson, J. Wurman, and P. M. Markowski, 2008a: Single- and dual-Doppler analysis of a tornadic vortex and surrounding storm-scale flow in the Crowell, Texas, supercell of 30 April 2000. *Mon Wea. Rev.*, **136**, 5017-5043.

Marquis, J., Y. Richardson, J. Wurman, P.M. Markowski, and D. Dowell, 2008b: Mobile radar observations of tornadic supercells with multiple rear-flank gust fronts. Preprints, *24th Conf. on Severe Local Storms*, Savannah, GA, *Amer. Meteor. Soc.*, 19.3

Rotunno, R., and J.B. Klemp, 1985: On the rotation and propagation of simulated supercell thunderstorms. *J. Atmos. Sci.*, **42**, 271-292.

Skinner, P.S., and C.C. Weiss, 2008: Observations of storm scale boundary evolution within the 23 May 2007 Perryton, TX supercell. Preprints, *24th Conf. on Severe Local Storms*, Savannah, GA, *Amer. Meteor. Soc.*, 4.3

Tanamachi, R.L., H.B. Bluestein, W.C. Lee, and M. Bell, 2006: Progress toward improved Ground-Based Velocity Track Display analysis of high-resolution radar data collected in tornadoes. Preprints, *23rd Conf. on Severe Local Storms*, St. Louis, MO, *Amer. Meteor. Soc.*, P9.3.

Trapp, R.J. and C. A. Doswell, 2000: Radar data objective analysis. *J. Atmos. Oceanic Technol.*, **17**, 105-120.

Weiss, C.C., J.L Schroeder, J. Guynes, P. Skinner, and J. Beck, 2009: The TTUKa mobile Doppler radar: Coordinated radar and in situ measurements of supercell thunderstorms during Project VORTEX2. Preprints, *34th Conf. on Radar Meteorology*, Williamsburg, VA, *Amer. Meteor. Soc.*, 11B.2

Wicker, L.J., and R.B. Wilhelmson, 1995: Simulation and analysis of tornado development and decay within a three-dimensional supercell thunderstorm. *J. Atmos. Sci.*, **52**, 2675-2703.

Wurman, J, Y. Richardson, C. Alexander, S. Weygandt, and P.F. Zhang, 2007: Dual-Doppler and single-Doppler analysis of a tornadic storm undergoing mergers and repeated tornadogenesis. *Mon. Wea. Rev.*, **135**, 736-758.

Figure 1: Photograph of the Dumas, Texas supercell. Photo taken at 23:01 UTC looking west.

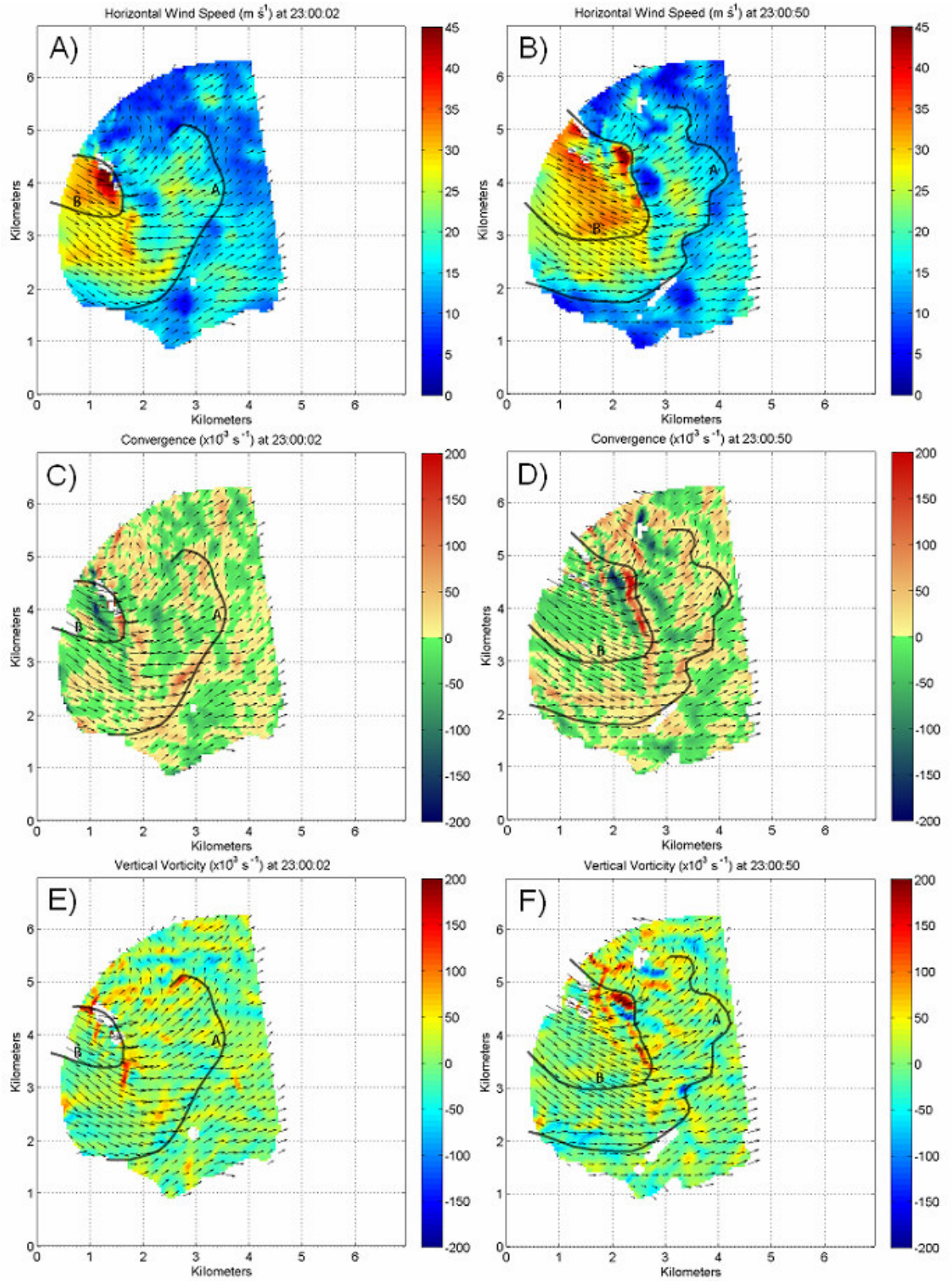

Figure 2: Dual-Doppler syntheses of wind speed (m s^{-1}) (A, C), convergence (x10^3 s^{-1}) (B, D), and vorticity (x10^3 s^{-1}) (C, E) in the Dumas supercell at 23:00:02 and 23:00:50 UTC. Labeled, bold lines represent RFGF positions.

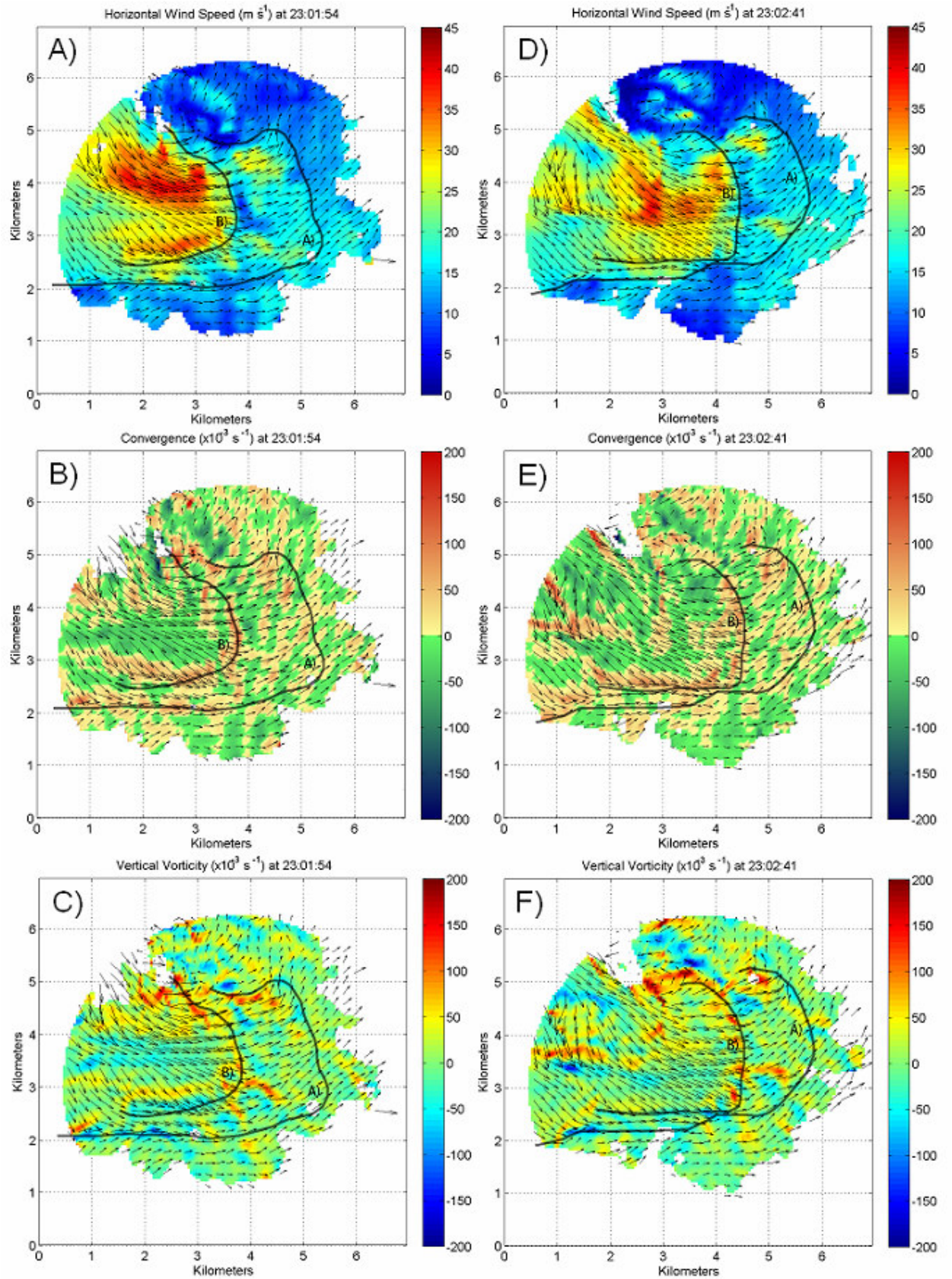

Figure 3: Same as Fig. 2, but for 23:01:54 and 23:02:41 UTC.

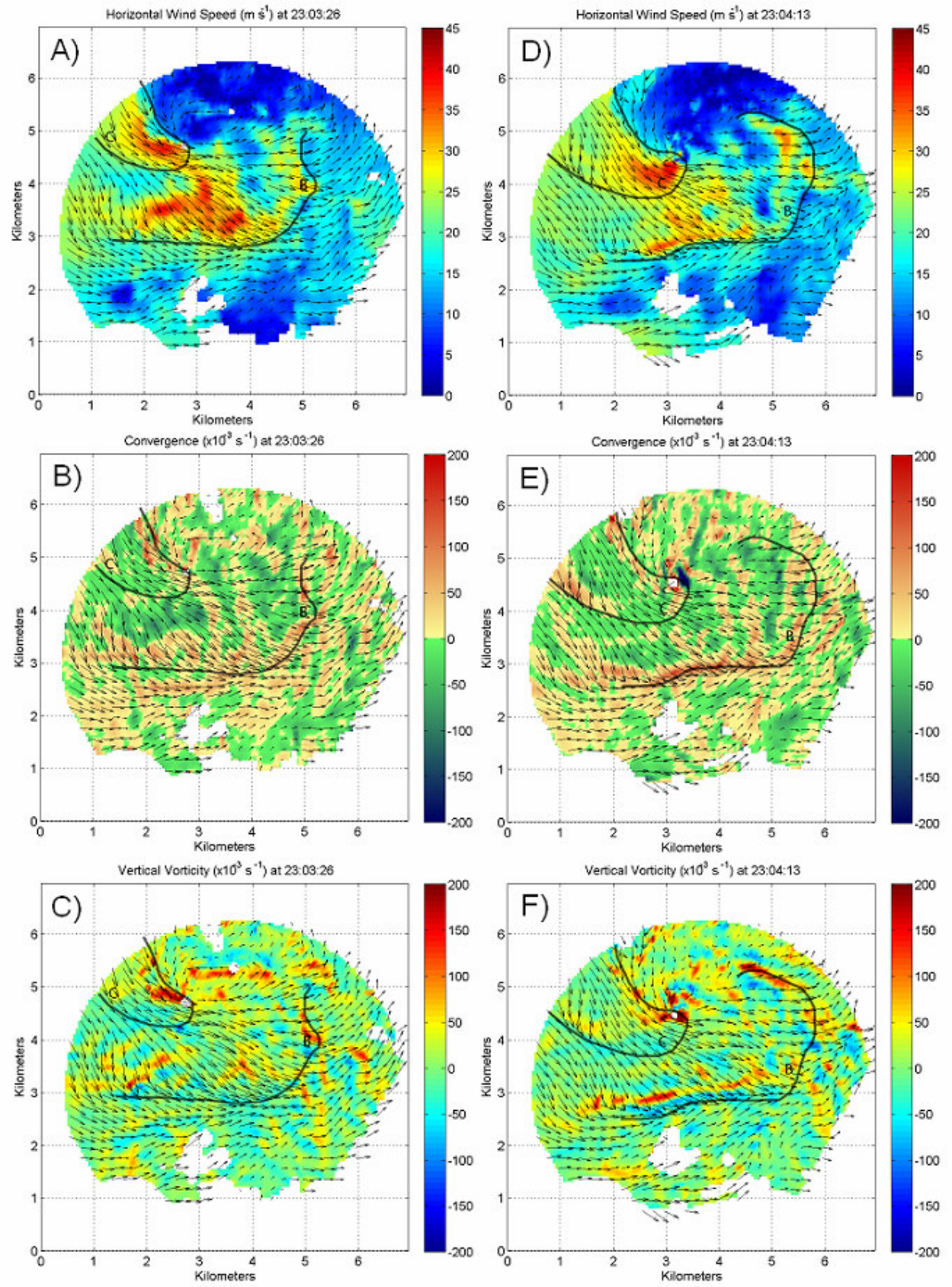

Figure 4: Same as Fig. 2, but for 23:03:26 and 23:04:13 UTC.

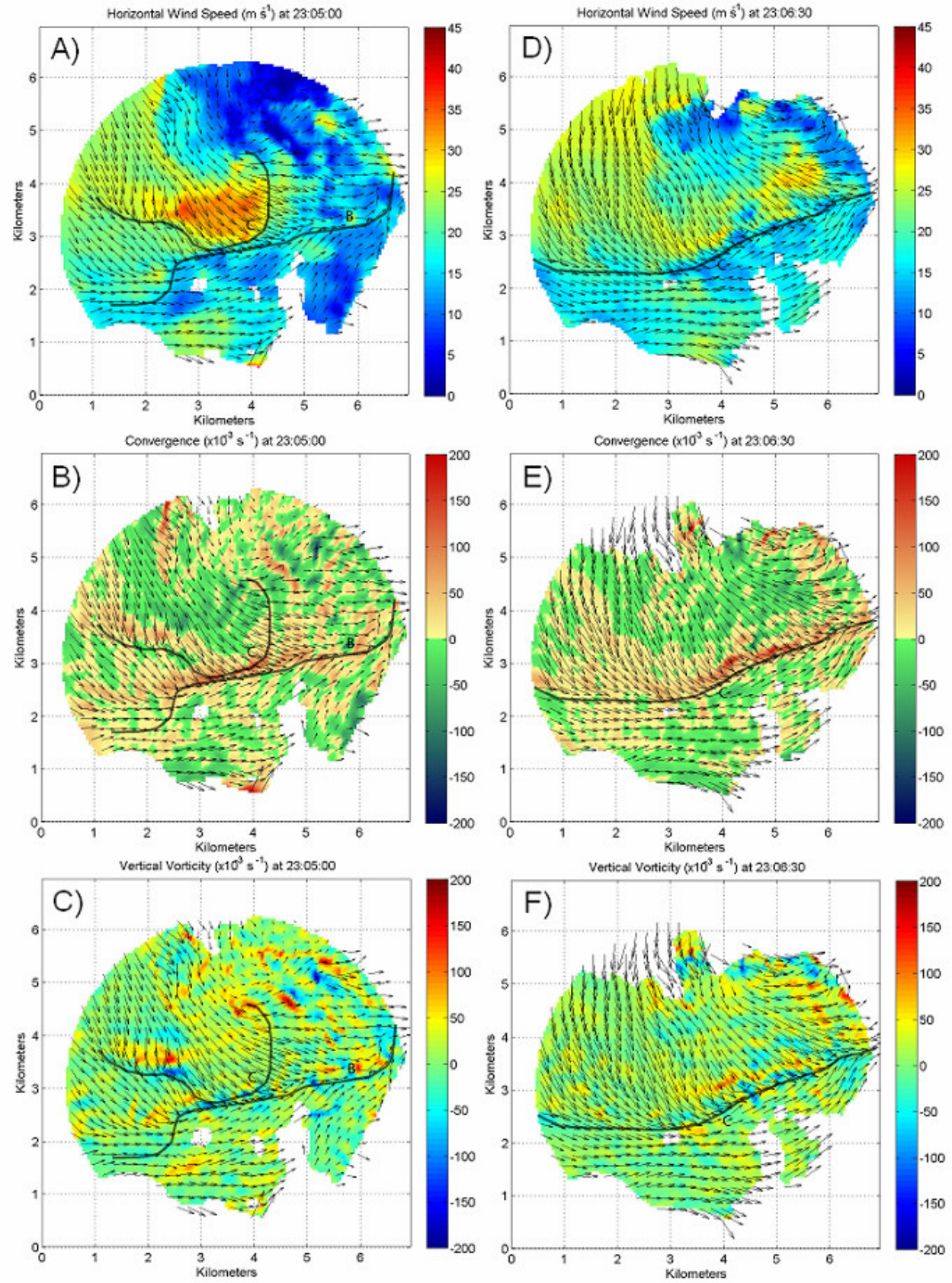

Figure 5: Same as Fig. 2, but for 23:05:00 and 23:06:30 UTC.

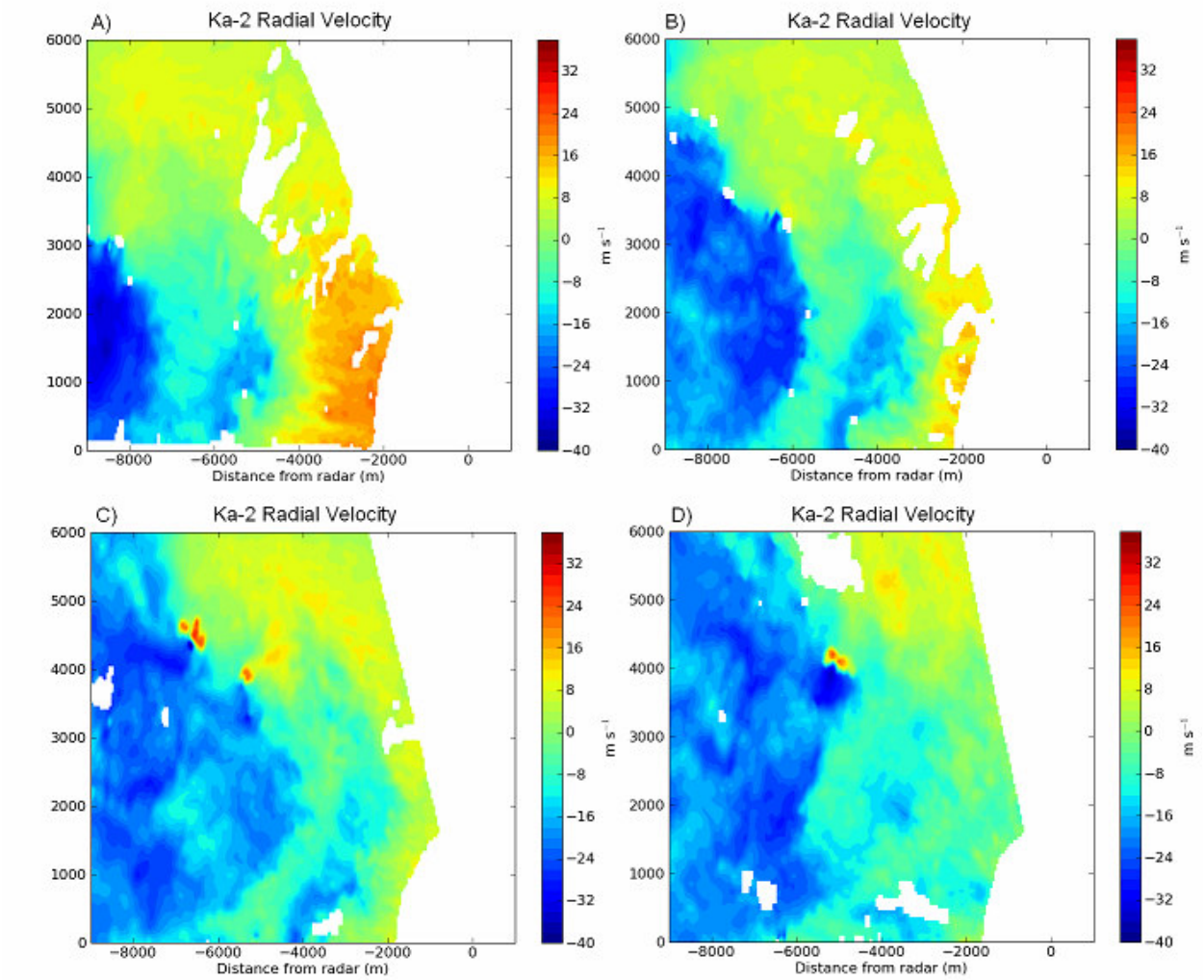

Figure 6: Objectively analyzed radial velocity (m s^{-1}) from the Limon, CO supercell at (A) 23:32:33, (B) 23:34:38, (C) 23:36:33 and (D) 23:38:26.